A STUDY OF THE DECIMETRIC EMISSION AND POLARIZATION OF CENTAURUS A

By B. F. C. Cooper,* R. M. Price,† and D. J. Cole*

[*Manuscript received June* 25, 1965]

Summary

The results of a study of Centaurus A in the wavelength range 6–74 cm are presented. From observations at 11, 21, and 31 cm the intrinsic polarization and Faraday rotation have been determined for much of the source.

Of the two sources that form the central component, the north-following source is strongly polarized at wavelengths shorter than about 31 cm. The south-preceding source is 3% polarized at 6 cm and not more than 3% polarized at 11 cm.

At 11 and 21 cm the degree of polarization in extended regions of the source is typically 10–20% and in places as high as 40%. The orientation of the intrinsic polarization is quite uniform over large areas but appears to bear no constant relationship to the axis of symmetry of the source.

In general the rotation measure varies slowly over the source, and values lie in the range -36 to $-84\ \mathrm{rad/m^2}$, with most values lying between -50 and $-70\ \mathrm{rad/m^2}$. Possible relationships between Faraday rotation and depolarization effects are discussed.

All parts of the source have an essentially constant spectral index of $-0\cdot6$ at decimetric wavelengths. The central component contributes approximately 22% of the total flux density, the remainder being equally divided between the northern and southern extended sources.

I. Introduction

Centaurus A was one of the first of the "discrete" sources of radio emission to be identified. The intense central sources were detected, although unresolved, in 1947, and reported by Bolton (1948). Soon afterwards, more precise measurements with their cliff interferometer at 100 Mc/s allowed Bolton, Stanley, and Slee (1949) to tentatively identify the peculiar radio emission with an unusual optical object, NGC 5128. Continued measurements showed that the source actually consisted of two components, a region of intense radio emission thought to be less than 7′ in extent, surrounded by a lower brightness envelope of approximately 30′ (Stanley and Slee 1950).

As equipment and techniques improved, knowledge of the complicated brightness distribution of this radio source increased, although major changes were not effected in the picture derived from earlier observations. Mills (1953) reported that interferometry showed the intense source to be 5′ wide in the east–west coordinate, while increased sensitivity allowed the extended source in the same region to be traced out to more than a degree. Bolton *et al.* (1954) confirmed these results and traced the regions of low brightness, which were believed to be physically associated with the intense source, out to a total width of more than 2° in the east–west direction.

* Division of Radiophysics, CSIRO, University Grounds, Chippendale, N.S.W.

† Division of Radiophysics, CSIRO, University Grounds, Chippendale, N.S.W., and Mount Stromlo Observatory, Canberra.

Aust. J. Phys., 1965, **18**, 589–625

Position measurements were now accurate enough to consider the radio source as definitely identified with NGC 5128. Further measurements by McGee, Slee, and Stanley (1955) at 400 Mc/s, and by Piddington and Trent (1956) at 600 Mc/s, served to confirm that the general brightness distribution of the source was similar over a wide range of frequencies.

Further surveys at various frequencies showed the extent of the source in the north–south direction. Sheridan (1958) investigated Centaurus A at 85 Mc/s (3·5 m) using a 50′ pencil beam and showed that the source extended over some 8° in declination. Thus at the presently accepted distance of 4 Mpc the projected linear extent of the source is 600 kpc, a dimension that is large, but not exceptional for radio galaxies. Measurements by Shain (1958) at 19·7 Mc/s showed essentially the same structure as that found at 85 Mc/s. By this time, the general structure of the source had been determined, and further measurement was primarily for the investigation of the brightness distribution with the higher resolution instruments that were coming into use, and for the study of the brightness distribution as a function of frequency. Hindman and Wade (1959) studied the source at 1400 Mc/s and further confirmed the previously determined structure, their observations bearing "a remarkably close resemblance" to findings at lower frequencies. Wade (1959) interpreted previous investigations as indicating that the extended source of low brightness temperature was a "double" source of radio emission, with the intense source (and NGC 5128) lying approximately midway between the two peaks of the extended source. Bolton and Clark (1960) applied a similar analysis to their 960 Mc/s observations and derived a similar brightness distribution for the extended source.

Further interferometry by several groups showed the intense central component to be double also. As most of the interpretations were based on information obtained with east–west base lines only, they seemed consistent with an earlier suggestion that the central radio source was closely associated with the dark lane of obscuring matter clearly visible on plates of NGC 5128. However, Maltby (1961) showed the central component to consist of two sources, each of about 2′ diameter, separated by about 7′ in position angle 46°·5. Each source appeared to be slightly elongated in the direction of the line joining their centres. The ratio of brightness of the two sources was estimated to be of the order of 1·3 to 1·0, at 960 Mc/s.

With the greatly improved resolution of the Parkes 210 ft telescope it has proved possible to delineate fine details of the source structure and to reveal the previously unsuspected polarization and Faraday rotation that is associated with the radio emission (Bracewell, Cooper, and Cousins 1962; Cooper and Price 1962). In the following sections the results of a detailed study of the source at wavelengths of 74, 31, 21, and 11·3 cm are presented, together with some restricted observations at 6 cm. From the 31, 21, and 11·3 cm observations the distribution of intrinsic polarization and Faraday rotation over the source has been delineated.

South-eastern Extension

Observations in the southern part of the extended source have shown that the absolute intensity on the east-following side of the source is significantly higher than on the west-preceding side. Piddington and Trent (1956) traced this feature in a south-easterly direction until it merged with the Galaxy some 20° away. They speculated that it was in fact a bridge between our Galaxy and Centaurus A (a suggestion that was not unreasonable at a time when the estimated distance was 700 kpc, but is difficult to accept in view of the present accepted distance of 4 Mpc). Also Bolton and Clark (1960) suggested that the south-east extension in the declination range $-44°$ to $-48°$ was physically associated with Centaurus A, but they were unable to trace its full extent from their northern observing site in California.

Observations at 74 cm with the 210 ft telescope have verified the continuity of this feature down to the galactic plane and its large angular extent. The extent and placing of the feature make it highly probable that it is a galactic spur, similar to those observed in other parts of the sky but extending for some distance in front of Centaurus A before fading out. If there is radio emission physically associated with Centaurus A in this region, it should be possible to identify it with the aid of polarization and Faraday rotation measurements. Such measurements have not yet been carried out owing to the extremely low brightness temperatures encountered there. For the present we have chosen to establish a boundary on the eastern side of Centaurus A where the emission shows a shallow minimum before rising again towards the galactic plane.

Optical NGC 5128

The optical object associated with the radio source Centaurus A is NGC 5128, one of the five extragalactic objects in the sky brighter than sixth total photographic magnitude (de Vaucouleurs 1953, 1956). NGC 5128 appears, on a medium exposure plate (Plate 1) as an unresolved E0 type galaxy bifurcated by a very strong absorption lane lying approximately along position angle 120°. This lane becomes more diffuse at both ends and curves in a manner that would suggest it is wrapped around the edge of the bright regions of the object. The brightest portions of the object are more than 10′ in extent and on long-exposure, high-contrast prints can be traced out to 1° with a noticeable elongation along position angle 45°. Composite photographic techniques have been applied to the object by Johnson (1963) and the results indicate a helical or "corkscrew" structure extending 45′ in position angle 40° and some 30′ along position angle 220°. This structure seems to involve both the dust lane in the central part of the optical object and the faint optical extensions on either side of the bright source.

Studies of spectrograms of the object indicate a velocity of about 400 km/s (with respect to the centre of our Galaxy). Turbulence is noted in the dust lane, while the bright portions of the object appear to be rotating about an axis perpendicular to the dust lane (Burbidge and Burbidge 1959). The object is not resolved into stars although Sérsic (1958) has reported chains of stars or perhaps HII regions within the dust lane. From estimates of the absolute magnitudes of the observed regions and the probable absorption, Sérsic (1961) derives a distance of 4 Mpc and an absolute magnitude of $-20 \cdot 8$ for NGC 5128, in agreement with estimates derived from the observed radial velocity.

Polarization studies of NGC 5128 by Elvius and Hall (1964) have shown light in the region of the obscuring dark band to be up to 6% polarized with the E vector approximately parallel to the band. It is not clear whether this polarization is due to the absorption in the dark clouds or to the observation of optical synchrotron emission, although the former seems the more likely suggestion.

II. Observing Methods

The observing techniques used were essentially the same at all of the wavelengths. However, the variations in resolution of the telescope at different wavelengths and the sensitivity of the various receivers used governed the rates at which the source was scanned and the spacing of the scan tracks. In general the source was scanned in right ascension at fixed declinations. Because of the large extent of the source in declination, right ascension scans could be kept shorter and receiver base-line drifts were more easily detected and corrected. Two sets of declination scans, at $13^h 19^m 30^s$ and $13^h 24^m 00^s$, were used for checks on both the brightness distribution and the polarization parameters determined with the right ascension scans.

To determine the intensity and polarization of the source each scan was repeated six times, with the feed of the telescope in a different orientation each time. The interval between feed angles was 30°, so that for each set of scans the feed angles used normally were 0°, 30°, 60°, 90°, 120°, and 150°. In the context of the altazimuth mounting of the 210 ft telescope, a feed orientation of 0° corresponds to the electric vector of the feed horn lying in the vertical plane containing the beam axis, while increasing feed angles imply anticlockwise rotation of the feed looking outwards along the beam. The position angle of the electric vector projected on the sky is then equal to the feed angle plus the parallactic angle, where the parallactic angle is the position angle of the vertical circle of the telescope measured east of north.

Since Centaurus A transits close to the zenith at Parkes and the parallactic angle changes rapidly near the zenith, scans were taken at large hour angles whenever possible so that correction for changes of parallactic angle would be small within the set of scans. When observations were taken close to transit, the separation of the feed angles was adjusted so that the resulting position angles of observation were very nearly 30° apart.

Scans were extended on either side of the source until it became apparent that the base level had been reached, or to a point related to the predetermined base level. On the preceding (early right ascension) side this was easily done. However, on the following side, particularly for the southern part of the source, confusion with the galactic spur in the region made the selection of a base level for the source more complicated and introduced a small uncertainty in the level of brightness temperature contours near that area.

The average of the six scans within a set was used to determine the brightness distribution along each scan track, while plots of feed (or position) angle versus intensity for individual points along the track were used to determine the polarization parameters for the given point at the observing frequency. Corrections for time constant and base line were applied to the intensity values where necessary, and a sine wave was then fitted by eye to the six intensity values plotted.

Many regions were further investigated for polarization using a feed-rotation technique. In these observations, the feed was rotated through 300° and back while the telescope was tracking a given point in the source. Similar rotations were taken at the same hour angle and declination (to ensure the same ground radiation effects) at points off the source. Rotations could be integrated to give a more accurate result than the scans at discrete feed angles provided, and were not prone to the same baseline effects that might result if the background were polarized in some unknown manner.

III. Total Emission and Polarization–Brightness Temperature Calibration

The measurement of the flux densities and brightness temperatures of partially linearly polarized sources has been discussed by Westerhout *et al.* (1962), and we follow their definitions and terminology with some variations. The isophotes presented in the following sections are of full-beam brightness temperature, which is equivalent to the aerial temperature that would be observed if the aerial received energy only within the confines of its full beam and had zero response elsewhere. The extent of the full beam is a somewhat arbitrary quantity, but it is taken here to extend out to a distance from the beam axis at which the aerial power response is not more than a few tenths of 1% of its maximum value.

The flux density of a source may then be obtained with good accuracy by integrating the contours of full-beam brightness temperature according to the relationship

$$S = (2k/\lambda^2)\int_{\text{source}} T_{\mathrm{B}}\,\mathrm{d}\Omega\,, \tag{1}$$

where k is the Boltzmann constant, λ is the wavelength, and T_{B} is the full-beam brightness temperature observed in the direction of the element of solid angle $\mathrm{d}\Omega$.

To establish a full-beam brightness temperature scale a point source of known flux density may be observed, in which case (1) reduces to

$$S = 2kT_{\mathrm{BP}}\Omega_{\mathrm{FB}}/\lambda^2, \tag{2}$$

where Ω_{FB} is the effective full-beam solid angle obtained by integrating the beam contours, and T_{BP} is the peak apparent brightness temperature of the point source, i.e. as smoothed by the beam. T_{BP} is then calculated from (2) to establish the relationship between receiver output and source brightness temperature.

Where a partially linearly polarized source is observed with a rotating linearly polarized feed, the apparent brightness temperature will vary between the limits $\max T_{\mathrm{B}}$ and $\min T_{\mathrm{B}}$, in which case the mean value $\frac{1}{2}(\max T_{\mathrm{B}} + \min T_{\mathrm{B}})$ is applied in (1). We define this mean value as the *full-beam total emission brightness temperature.* To specify the polarized component we define $\max T_{\mathrm{B}} - \min T_{\mathrm{B}}$ as the *full-beam polarization brightness temperature.* The degree of linear polarization p at that point is then given by

$$p = \frac{\max T_{\mathrm{B}} - \min T_{\mathrm{B}}}{\max T_{\mathrm{B}} + \min T_{\mathrm{B}}}.$$

In the present paper the adopted unit of flux density is $10^{-26}\,\mathrm{W\,m^{-2}\,(c/s)^{-1}}$, which will be referred to hereafter as 1 *flux unit.*

At all observing wavelengths, brightness temperature scales were determined as described above. A noise step coupled into the aerial feeder from an argon discharge tube was used as a transfer calibrator between the standard sources and the unknown sources. The receiver non-linearity was measured by applying this noise step in the manner described by Komesaroff and Mathewson (1962).

The standard source flux densities adopted in the following sections are close to the values derived by Conway, Kellermann, and Long (1963), but are modified slightly in the light of more recent work at Parkes and elsewhere. The characteristics of the receivers used at the various frequencies are summarized in Table 1, together with beam dimensions and the assumed flux densities of the reference sources.

TABLE 1

EQUIPMENT SUMMARY

Frequency (Mc/s):	406	960	1410	2650	5000
Receiver:					
Type	Crystal mixer	Crystal mixer	Parametric	Parametric	Crystal mixer
Bandwidth (Mc/s)	8	8	10	100	10
System noise temp. (°K)	350	400	105	180	650
Beamwidth at half intensity (min of arc)	48·0	20·0	14·0	7·35	4·1
Full-beam solid angle (sr)	$2{\cdot}08\times10^{-4}$	$3{\cdot}96\times10^{-5}$	$1{\cdot}83\times10^{-5}$	$5{\cdot}15\times10^{-6}$	—
Assumed flux densities ($10^{-26}\,\mathrm{W\,m^{-2}\,(c/s)^{-1}}$)					
Hydra A	135	64	45	23·5	12·4
Virgo A	560	285	210	120	76

IV. Observations at 74 cm

The receiver (Mackey 1964) used for the 74 cm observations was a crystal mixer type, which accepted two sidebands, each 8 Mc/s wide, centred on 396 and 416 Mc/s. Its sensitivity was more than adequate for observing the high brightness temperatures encountered in Centaurus A. The passband characteristic of this receiver was satisfactory for determining the isophotes of the source, but was not suitable for observing any polarization that might have been present, as the observations at shorter wavelengths showed that a differential Faraday rotation of about 250° was to be expected across the sidebands. However, some 74 cm polarization checks have been made independently by F. F. Gardner and A. G. Little (personal communications) using a receiver that accepted a single sideband only 4 Mc/s wide. The differential Faraday rotation across this bandwidth would cause no more than 10% depolarization in the case of Centaurus A. Their observations showed that the regions strongly polarized at short wavelengths were virtually unpolarized at 74 cm, either by internal depolarization in the source, by confusion effects in the larger beam at this wavelength, or by differential Faraday rotation across the telescope beam.

Scans were made at half-beamwidth intervals, and the isophotes constructed from them are presented in Figure 1. By comparison with the shorter wavelength maps much of the fine detail has been smoothed out by the increase in beamwidth to 48′. However, the foreground structure surrounding Centaurus A becomes relatively bright at 74 cm, and it is easier to distinguish the intensity rise that occurs in crossing

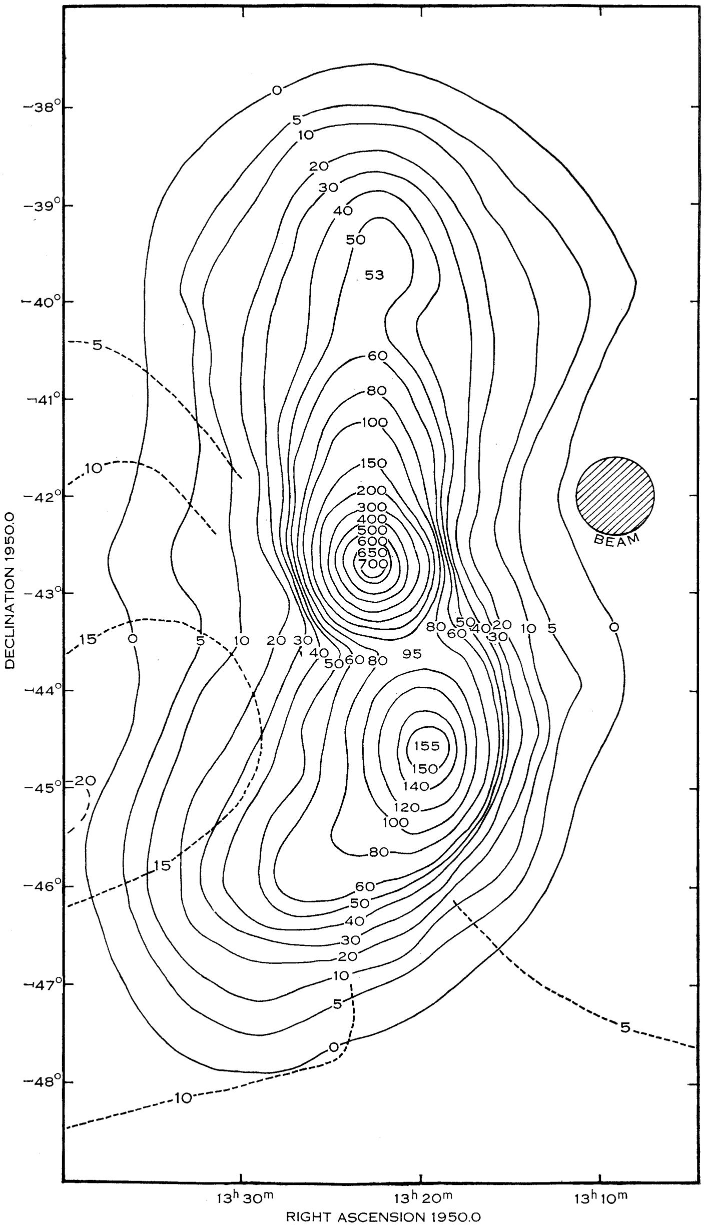

Fig. 1.—Isophotes of full-beam total emission brightness temperature at 406 Mc/s. Full-line contours show brightness temperature (in °K) above the estimated galactic foreground structure (indicated by the dashed contours). Epoch 1950.0. Observed with a 48′·0 beam.

the southern part of the source from west to east. As discussed earlier, we have tentatively concluded that this intensity rise is due to a galactic spur that extends upwards in a north-westerly direction from the galactic plane and fades out in front of Centaurus A. This spur was traced by several scans in the direction of the galactic plane, and its general structure was evident in more detail in the 400 Mc/s survey scans kindly made available by J. G. Bolton, F. F. Gardner, and M. B. Mackey. The dashed contours in Figure 1 show the estimated intensity of this spur above an arbitrary zero level, which is taken just outside the western boundary of Centaurus A. A fairly uniform intensity plateau was found in this region extending from declination $-37°$ to $-47°$.

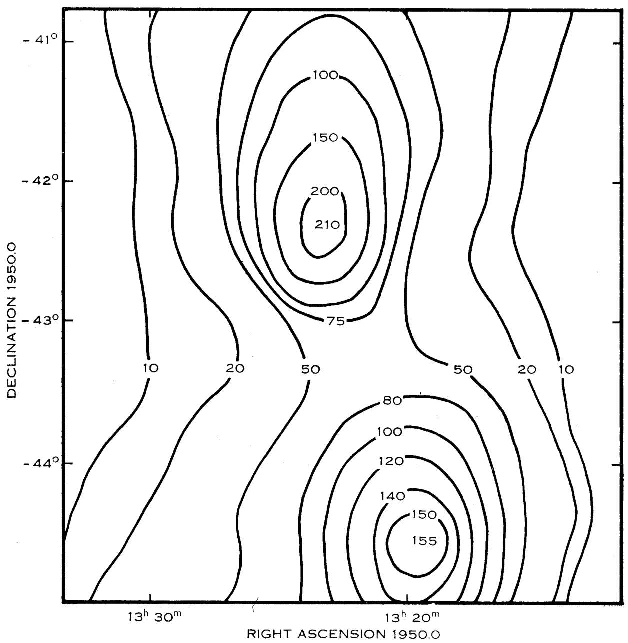

Fig. 2.—Isophotes of the extended source structure in the central region, derived by subtracting the estimated central component of flux density $595\times10^{-26}\,\mathrm{W\,m^{-2}\,(c/s)^{-1}}$ from the isophotes of Figure 1.

The aerial beam shape was determined to be circular within close limits with a half-intensity diameter of 48′. Its shape was accurately Gaussian down to the half-intensity point, but somewhat narrower than Gaussian below this intensity. Integration of the beam contours gave an effective full-beam solid angle of $2\cdot08\times10^{-4}$ sr. For a point source with a flux density of 1 flux unit, observed with a beam of these dimensions, the peak brightness temperature by equation (2) (Section III) was $0\cdot94$°K.

The contribution of the central component to the isophotes was determined by subtracting patterns of various peak intensities, corresponding to the central double source convolved with the main beam, until a set of residual contours, which were consistent with the known structure and spectrum of the extended source in this region, was obtained. After subtraction of a pattern of 550°K peak brightness temperature, corresponding to a combined flux of 595 flux units from the two central sources, the residual contours of Figure 2 were obtained. These are considered to be consistent with the structure observed at 21 and 11 cm after allowing for a 0·6 spectral index and the dilution effect of the 48′ beam. The flux contributions from the north, south, and central portions of the source, obtained by integrating the T_B contours, are listed in Table 2.

V. Observations at 31 cm

Observations at 31 cm were carried out using a total-power radiometer of the crystal mixer type. Both sidebands (each of 8 Mc/s bandwidth with centre frequencies separated by 20 Mc/s) were accepted by the receiver. With the 2 s output time constant used in the observations, the peak-to-peak fluctuations on the records were 0·6 degK of aerial temperature. The primary feed was a pyramidal horn, which was designed to illuminate the dish equally on both the E and H planes and to provide low ground radiation "spill-over".

Table 2

centaurus-a flux densities at 406 Mc/s

Region	Flux Density (10^{-26} W m^{-2} (c/s)$^{-1}$)	Fraction of Total (%)
North of centre	1075	39
Central component	595	22
South of centre	1070	39
Total	2740	100

At a wavelength of 31 cm, the half-power beamwidth of the telescope was measured to be 20′·0. With this resolution, a scan rate of 1°/min with a time constant of 2 s was adequate to follow the steepest intensity changes found in the extended portions of the source without distortion. A special survey was carried out over the central source, using slower scans and a calibration procedure that allowed its peak temperature to be compared with that of Virgo A.

Scans were placed 15′ apart in most parts of the source, following the same declination values used in the other wavelength surveys, whenever possible, for direct comparison.

The observed brightness distribution over the source at 31 cm is shown in Figure 3(*a*). Figure 3(*b*) shows the distribution of polarization brightness temperature and the observed directions of the E vectors of the polarized emission. Position angles for these E vectors are given in Table 3.

Polarization was measurable over some 30% of the source area, but by comparison with the shorter-wavelength maps it is apparent that depolarizing effects are beginning to operate rather strongly at this wavelength. However, there are several areas where the degree of polarization is still as high as 10% and one area

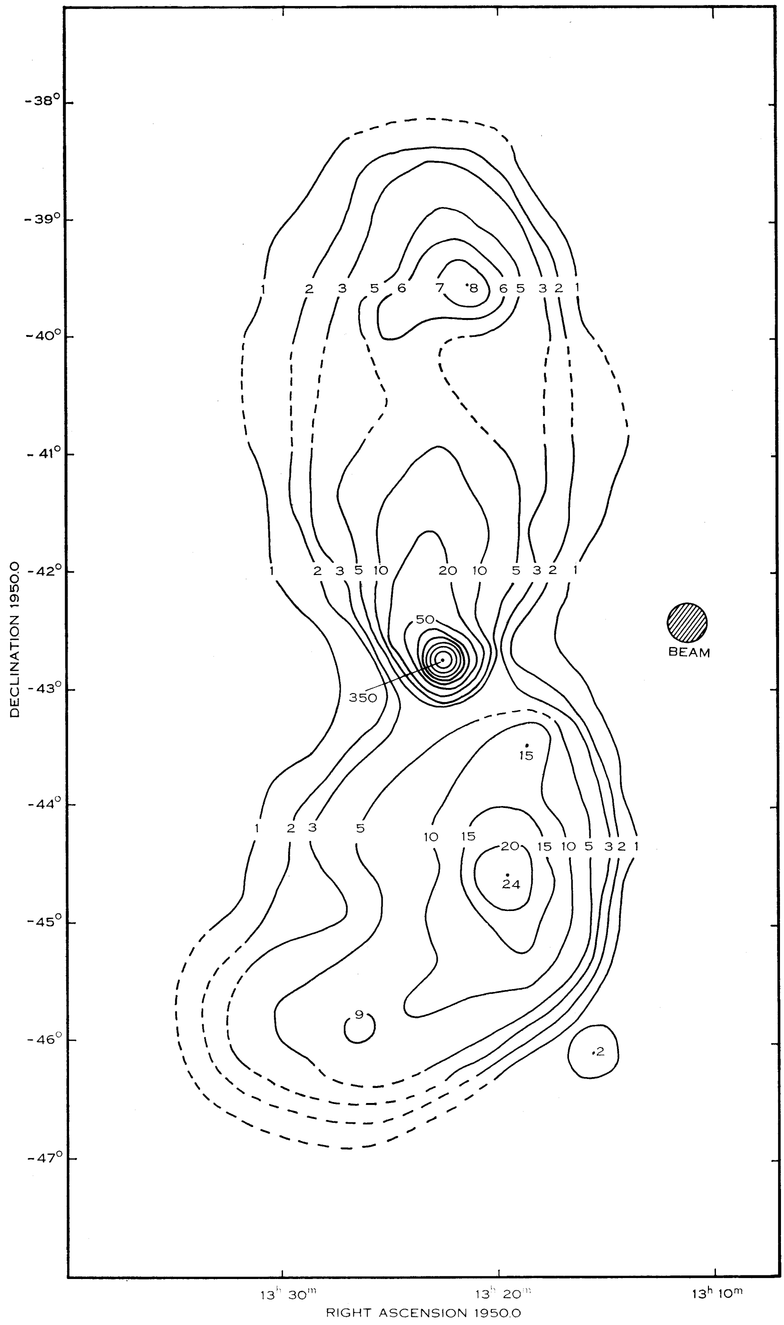

Fig. 3(*a*).—Isophotes of full-beam total emission brightness temperature at 960 Mc/s (in °K); beamwidth 20′·0 at half intensity. Contour interval for the central component is 50 degK.

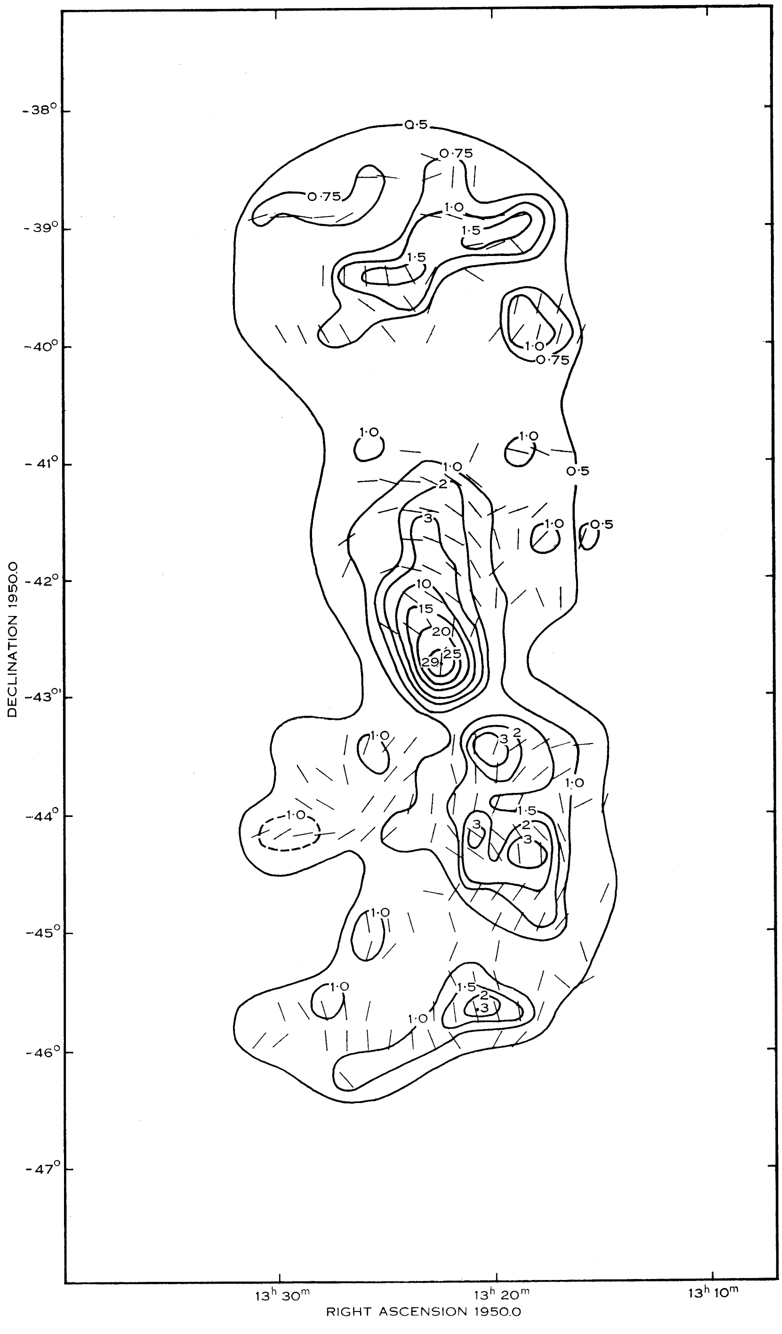

Fig. 3(*b*).—Isophotes of full-beam polarization brightness temperature at 960 Mc/s (in °K). The position angles of the observed *E* vectors of the polarized emission are indicated by short lines.

TABLE 3

CENTAURUS-A POLARIZATION POSITION ANGLES IN DEGREES AT 960 Mc/s

Add 20 s to indicated minute of right ascension

Declination 1950.0	Right Ascension 1950.0																
	13^h15^m	16^m	17^m	18^m	19^m	20^m	21^m	22^m	23^m	24^m	25^m	26^m	27^m	28^m	29^m	30^m	31^m
−38° 26′									73								
36									108		80	89?					
56					104	96	71	74	80				117	94	84	89	104
−39° 11′					47	112	100										
26							60		150	30	10	3	178	0			
41			165	166	164				158	35		56					
56		158	165	165	145	140			153		40		30	30	25	30	
−40° 56′			83	66	77		156			85							
−41° 11′							50	56	66	86	75	95					
26				134	108	118	41	56	76	82	102						
41		161		137	175		14	38	59	68	88		123				
56						136	29	48	63	76	107		157				
−42° 11′			0	20	133	175	34	52	56	53							
26							159	177	32	53	57						
Central peak								0±5									
−43° 26′		96	106	123	126	161	175	173		142	141	161	171				
41			122	130	140	175	0	15		132	140		14	50	30		
56	162	115	10	93	155	162	170	174	176	165	146	147		58	58		
−44° 11′			22	37	32	50	55	35	167		131	134	122	97	102	122	112
21			12	2	6	32	57	57		104	107						
41	160		153	144	146	145	150	148	80	75?	75?						
56			141	156	156	156		16		16	6	6					
−45° 11′		19				169		157			139	164					
26		120	50	160		17	11	23									
41				158?	8	15	13	8	0				5	16	33	21	
56					135	150?		34	21	5	172	3	0	7		132	140
−46° 16′													42				

near right ascension $13^h 24^m$, declination $-42° 15'$, where the degree of polarization is as high as 20%.

In Table 3 and the following Tables 4, 5, and 6, the position angles have been tabulated at the points where observations were made. It was considered undesirable to smooth and interpolate the angles to neat minutes of right ascension and degrees of declination (1950.0 epoch), as in many places rapid changes of angle occurred in a short distance.

VI. Observations at 21 cm

Observations of the source at 21 cm wavelength were carried out using a switched radiometer with a degenerate parametric r.f. preamplifier (Gardner and Milne 1963). Its centre frequency was 1410 Mc/s with a bandwidth of 10 Mc/s. With the 2 s time constant used in the observations, the peak-to-peak noise fluctuations observed were 0·2 degK of aerial temperature. Most of the observations were carried out using combined feeds, which allowed simultaneous observations at both 21 and 74 cm. However, a few observations were carried out with a single 21 cm feed. In all cases, the feeds were designed for similar illumination of the reflector in both the E and H planes, the primary feed response being 14 dB at the edge of the reflector surface to minimize ground effects. Calibrator sources were observed with all of the feeds used to ensure accuracy in calibrations.

At 21 cm, the measured beamwidth of the telescope, to half-power points, was 14′·0 with a high degree of circular symmetry. With this beamwidth and a 2 s time constant for the receiver output, a scan rate of 1°/min allowed 7 time constants per beam passage over a point, and permitted accurate determination of the brightness distribution over the track of the scan.

Scans were spaced at 15′ intervals in the extended portions of the source, this spacing being reduced to 10′ in regions of higher brightness, and further reduced to 7′ in the region of the central component. The scans were extended from $13^h 05^m$ to $13^h 40^m$ right ascension to allow accurate determination of the base levels. A slight change in aerial temperature with changing zenith angle due to ground spill-over was observed, but this was assumed to be linear over the small zenith-angle ranges for any one scan and its effect was removed in the reduction of the records. To determine the polarization parameters of this spur region, declination scans at six feed angles were made from $-42°$ to $-48°$ at right ascension $13^h 38^m$. In analysis of these parameters it was assumed that their end-points were in regions that exhibited negligible polarization at 1410 Mc/s. The region was found to be slightly polarized with average polarization temperatures of 0·2°K and a few values up to 0·4°K. At intermediate points along the right ascension scans that were terminated in this spur region, a correction vector was applied whose amplitude was taken to vary linearly from zero at right ascension $13^h 12^m$ to the measured amplitude at $13^h 38^m$. Notwithstanding these corrections, it is possible that residual uncertainties due to foreground polarization averaging 0·2 to 0·3 degK remain on the south-following side of the source. Since the foreground polarization may compound with the source polarization at arbitrary angles, the observed polarization may be modified in amplitude or orientation, or partly in both, to an extent appropriate to the amount of foreground polarization estimated above.

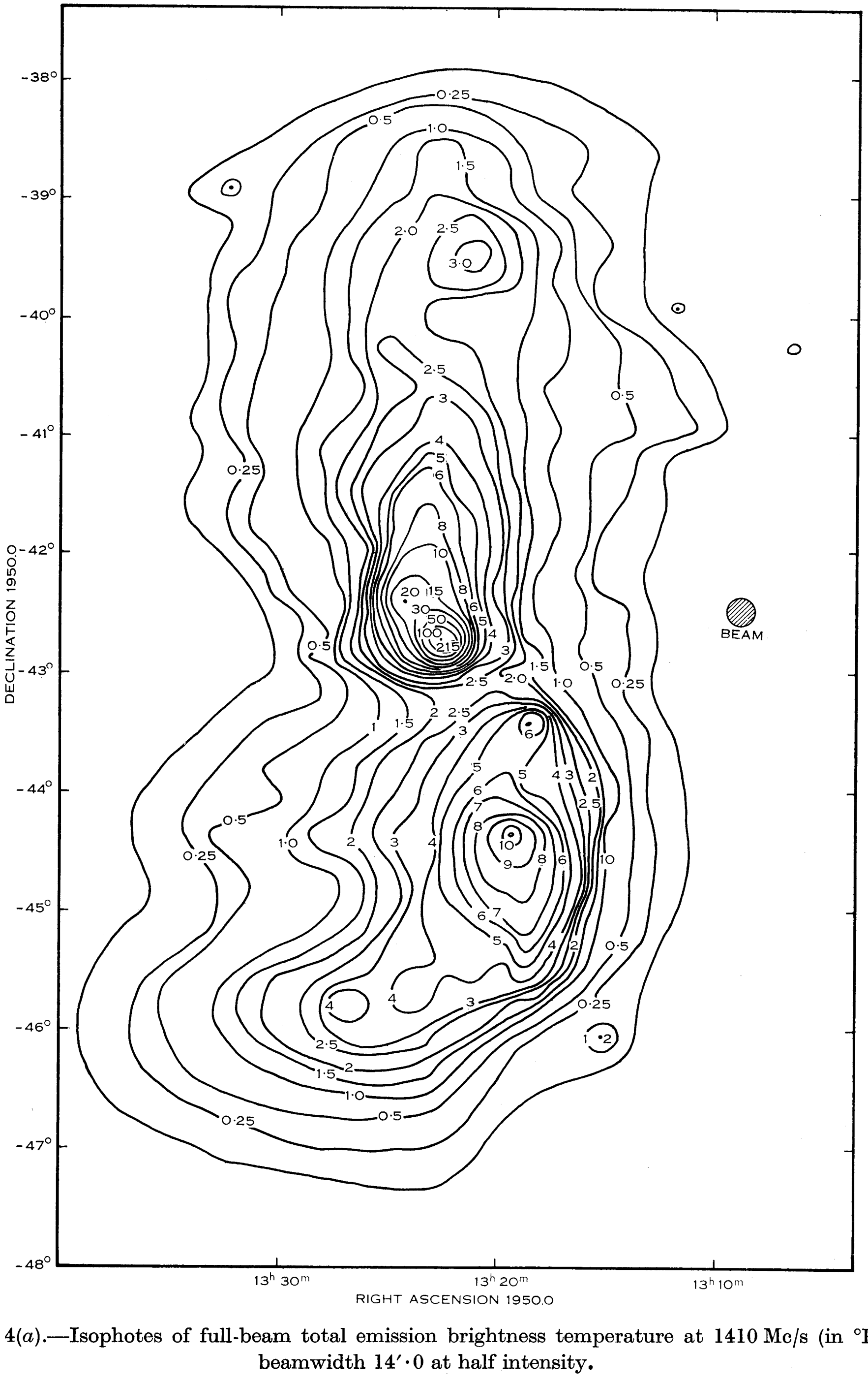

Fig. 4(*a*).—Isophotes of full-beam total emission brightness temperature at 1410 Mc/s (in °K); beamwidth 14′·0 at half intensity.

Figure 4(a) shows the observed brightness distribution over the source at 21 cm, while Figure 4(b) shows the distribution of polarization brightness temperature

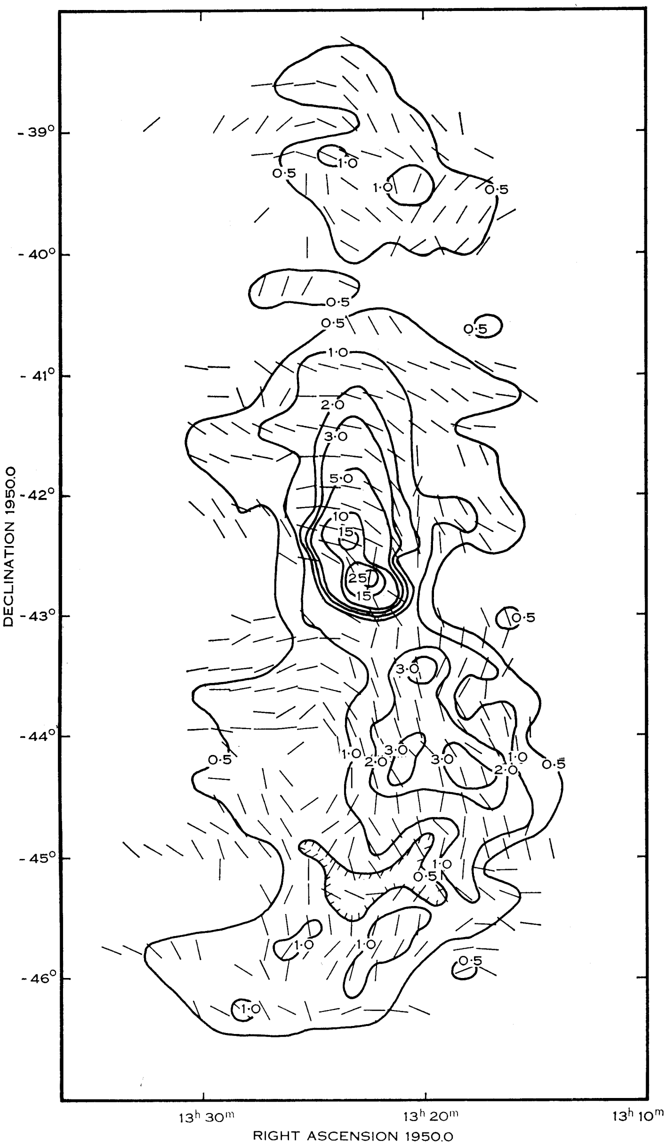

Fig. 4(b).—Isophotes of full-beam polarization brightness at 1410 Mc/s (in °K). Short lines indicate the observed directions of the E vectors.

across the source and the observed directions of the E vectors of the polarized emission. Position angles for these E vectors are given in Table 4. The peak in Figure 4 near right ascension $13^{\mathrm{h}}\,18^{\mathrm{m}}$, declination $-43°\,26'$, is due to an extraneous source,

TABLE 4

CENTAURUS-A POLARIZATION POSITION ANGLES IN DEGREES AT 1410 Mc/s

Add 20 s to indicated minute of right ascension

Declination 1950.0	Right Ascension 1950.0																			
	$13^h 15^m$	16^m	17^m	18^m	19^m	20^m	21^m	22^m	23^m	24^m	25^m	26^m	27^m	28^m	29^m	30^m	31^m	32^m	33^m	34^m
−38° 16′									62											
26									55											
36								30	49	73	94	96								
46									45											
56				11	41	36	21	26	45	66	11	41	145	20	146					
−39° 11′			78		55	40	61	74	63	66	73	105	95							
26			125	135	145	160	25		45	5?	1?									
41		120	145	150	145	150	50	50	63	30				135	110	75				
56		118	144	134	115	124	154		64		0									
−40° 16′		154?							69		150	160	160							
36							35	30	50											
56		75	60	70	70	70	65	75	78	75	70	60	55		90	85				
−41° 11′	53?	82	72	52	52	62	62	72	76	91	90	150	10	20	0					
26			86	76	54	56	49	66	79	81	81		66	56	56	56				
41			24	19		3	55	55	82	86	91	116	80	80	67	69				
56						156	39	59	80	80	102									
−42° 06′		35	35	30	15	178	19	63	75	82	95	178	39	69	34	49				
16		60	60	45	10	174	25	50	75	77	75	30?		29	29					
24		36	36	15	5	15	36	35	66	71	76									
32					30	0	25	170	40	60	80	60								
38								164	24											
44								173*												
52							55	25												

−43° 01′		19	24		12	7	34	31	60	32	44		99	69						
11		160	170	173	175	7	175	164	65	90	100	103	105	120	95					
26		151	161	156	13	15	19	17	59	102	116	110	97	107	107	110				
36	34	30	27	25	15	13	10	10	42	33	130	120	85							
48			175	155	160	15	20	20	56	75	80	105	100	100	100	90				
56	0	12	27	36	20	14	17	18	20	36	96	96	90	87	80	93	96	96	102	
−44° 06′		8	31	50	33	45	45	28	22	8		126			44					
21			16	17	14	25	32	15	175			129	7		85					
33			38	15	170	9	7	174	151	150	125	36	18	22	30					
46	160	15	12	175	46	15	25	30	130	126		30	41	32	56	60				
56	12	3	0	168	172	30	32	32	170	146	6	24	40	38	18	30	56	60	48?	
−45° 06′		90	80	175	170	160	90?	35	16	150	0									
18	89	70	51	51	36	146	146	97	66	62	2	158	29							
32	82	52	87	127		172	169	162	177	7	10	7								
36		62			93	172	170	165				15								
46			86	98		140	155	153	145	134	144	157	166			12	27	44	64	69
56			63	110				175	162	150		170	25	60						
−46° 16′						68	83	90	110	98	18		30	49	63	23				
26									63											

* North-following central source.

which is described separately in Section XIII. Other minor point sources may be noted around the periphery of Centaurus A.

Figure 5 shows the distribution of the source polarization at 1410 Mc/s in percentage groups. Apart from the highly polarized region just north of the central component, it is seen that highly polarized regions are concentrated towards the edges of the source. This is to be expected as the depth of the emitting regions should be least near the edges of the source.

VII. Observations at 11·3 cm

The receiver used for the 11·3 cm observations was a parametric type (Cooper, Cousins, and Gruner 1964) that accepted a band of frequencies 100 Mc/s wide centred on 2650 Mc/s. A 2 s output time constant was used during most of the observations, allowing the telescope to be driven at up to $0°\cdot5$/min without significant loss of detail in the source. With this time constant the peak-to-peak output fluctuations were of the order of 0·2 degK. In view of the low signal-to-noise ratio encountered over much of the extended regions of Centaurus A, the 11 cm observations were limited to areas where significant polarization was observable at 21 cm.

Figure 6(*a*) shows the isophotes of total emission observed at 11·3 cm while Figure 6(*b*) shows the distribution of polarization brightness temperature and the observed directions of the E vectors. Position angles for these E vectors are given in Table 5(*a*). Details of the central structure are shown in expanded form in Figures 7(*a*) and 7(*b*). Polarization position angles for the central region are tabulated in Table 5(*b*). The extraneous sources that are present in Figure 4 have been removed from Figure 6.

At 11 cm the beam shape was not quite circular, being $7'\cdot5$ wide in the E plane and $7'\cdot2$ wide in the H plane at half intensity. Its effective full-beam solid angle was determined to be $5\cdot15\times10^{-6}$ sr, so that by equation (2) (Section III) the observed peak brightness temperature of a source of 1 flux unit would be 0·9°K.

In observing the polarization of the central component, corrections were made for spurious instrumental effects produced by the elliptical beam section. These occurred whenever one of the central sources was situated on the steep sides of the aerial beam pattern. Corrections were made by subtracting polarization vectors determined from the measured beam sections in the E and H planes. Another minor correction was necessitated by a small variation of aerial gain with feed orientation. This produced a spurious polarization component of 1·3% of the source intensity with its maximum always coinciding with vertical polarization of the feed. When corrected for these effects, the contours for the total emission and the polarized emission of the central region are as shown in Figure 7. The centres of the north-following and south-preceding sources are marked A and B respectively.

The north-following source is 14% polarized at this wavelength and its polarized flux shows a well-defined pattern corresponding to the beam shape. At distances more than one beamwidth from A, the polarization vectors swing abruptly to the general north–south orientation that applies to the surrounding areas. As shown later, this cannot be due to a change in Faraday rotation, but must be due to a sudden shift in the magnetic field orientation at the boundary of the north-east source. A

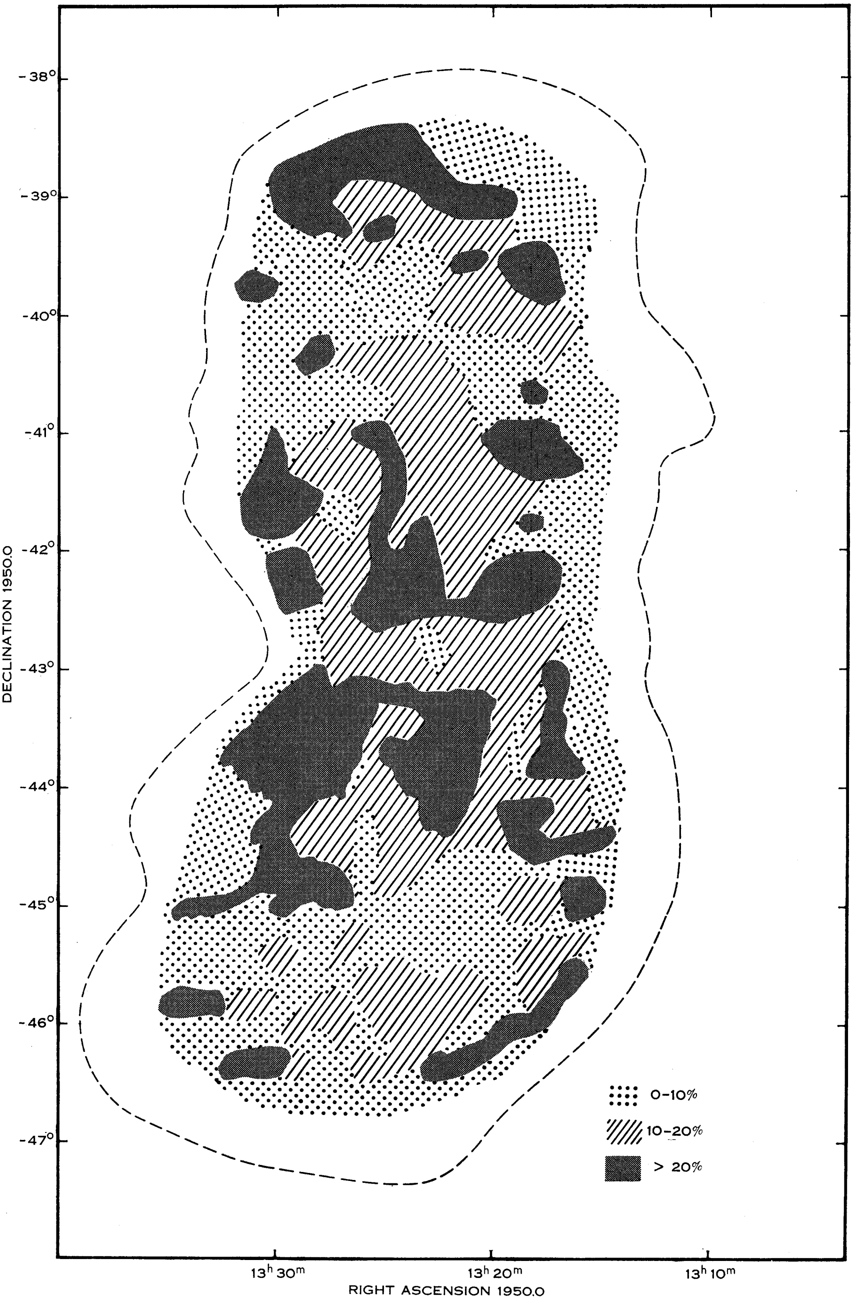

Fig. 5.—Distribution of the source polarization at 1410 Mc/s in percentage polarization groups 0–10, 10–20, and greater than 20%.

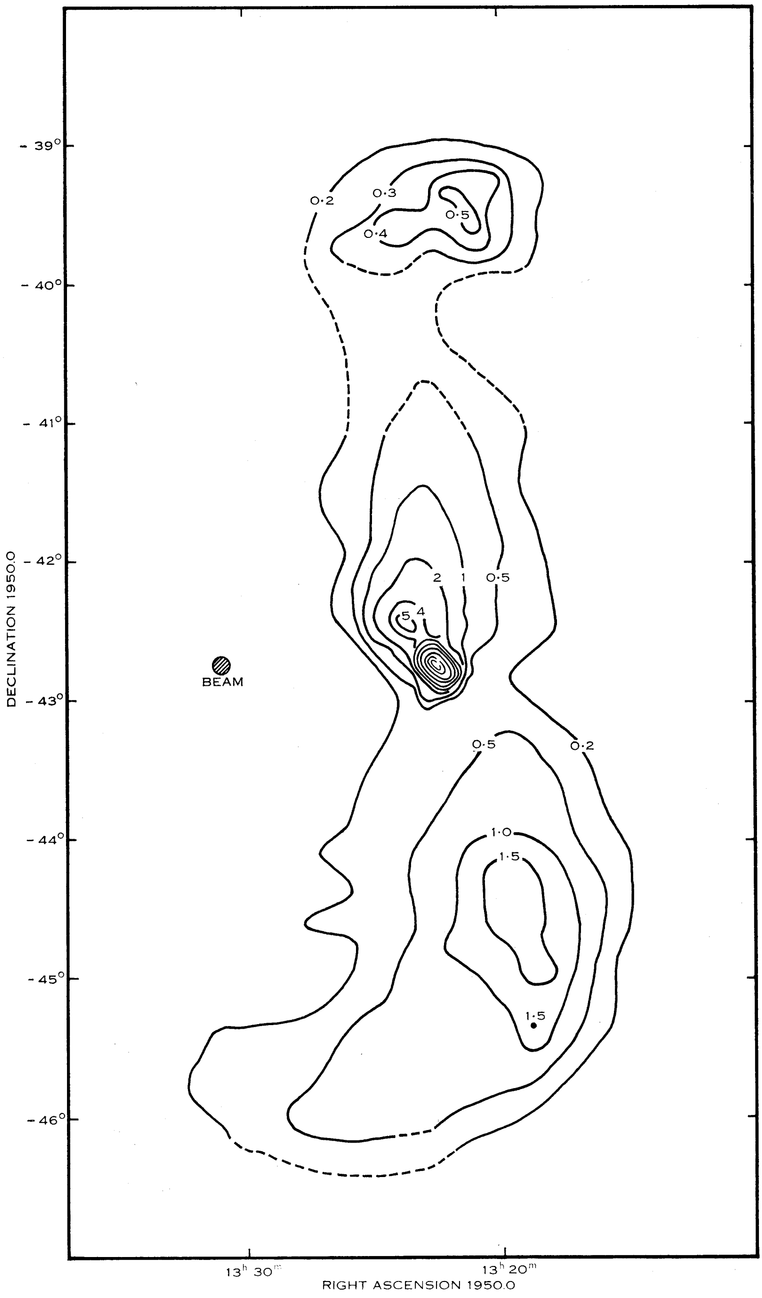

Fig. 6(*a*).—Isophotes of full-beam total emission brightness temperature at 2650 Mc/s (in °K); beamwidth 7′·4 at half intensity. Details of the central region are shown in Figure 7.

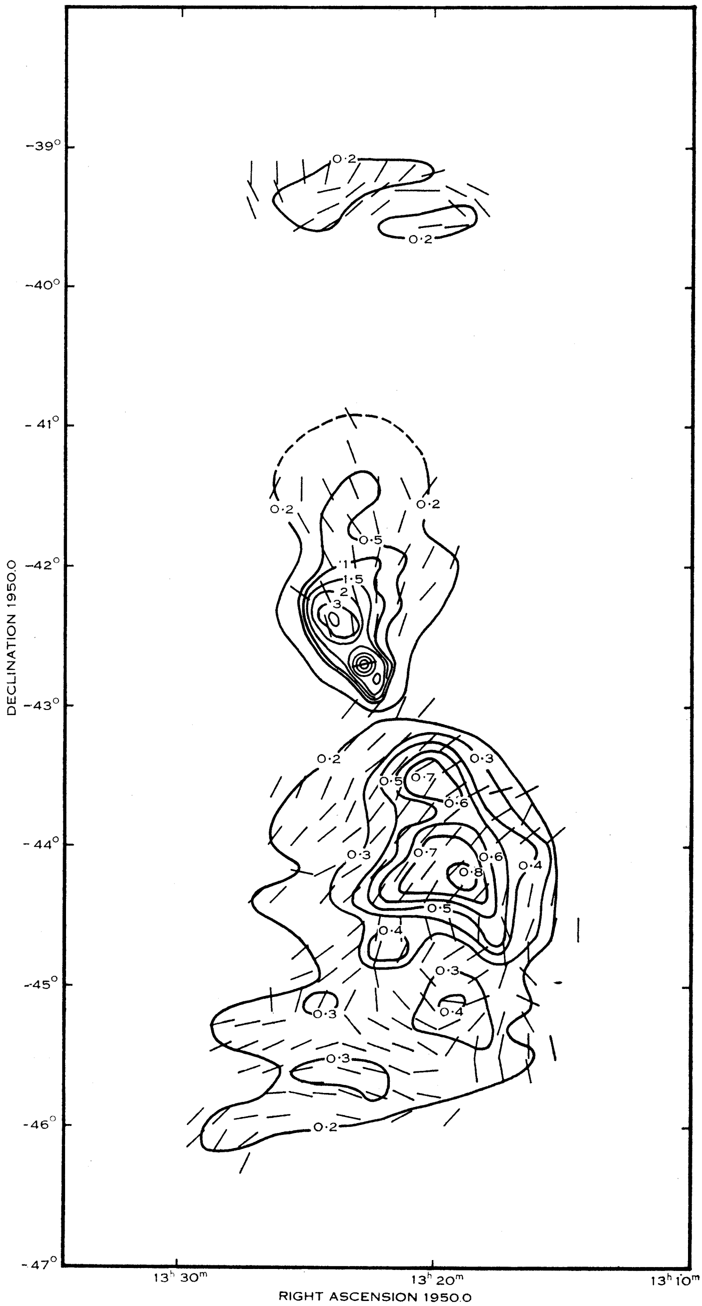

Fig. 6(*b*).—Isophotes of full-beam polarization brightness temperature at 2650 Mc/s (in °K). Short lines indicate the observed directions of the *E* vectors.

TABLE 5

CENTAURUS-A POLARIZATION POSITION ANGLES IN DEGREES AT 2650 Mc/s

(*a*) *Outer Regions*

Add 20 s to indicated minute of right ascension. Boldface numbers also observed by the rotating-feed method

Declination 1950.0	Right Ascension 1950.0														
	$13^h 15^m$	16^m	17^m	18^m	19^m	20^m	21^m	22^m	23^m	24^m	25^m	26^m	27^m	28^m	29^m
−39° 11′·0						105?	135?	150	135	168?	5?	0?	0?		
18′·5				65?	65?	90	90	108	123	100		20	25	15	
26′·0				40?	50?			130	130	114			20		
33′·5					95	90			125	120	120				
41′·0					96				120						
56′·0									95						
−40° 56′·0									30						
−41° 11′·0									**19**						
26′·0						145	23	0	**19**	26	176	160			
41′·0					128?	68?	162	12	25	34	35				
	See Table 5(*b*) for central region														
−43° 01′·0					128	138	158	143	143	153	143	143			
06′·0						158	168	158							
11′·0						149	164	154	164	179					
16′·0					125	135	135	135	140						
26′·0					124	142	139	124							
36′·0		116	100	110	125	150	160	150	145	160	160	154			
46′·0		119	119	119	128	145	150	145	144	135					
56′·0	135	135	135	149	**140**	142	140	139	132	126	137	140			
−44° 03′·5		114	134	143	143	153	153	143	133	144					
11′·0		150	153	140	135	145	147	140	135	115	80				
21′·0	140	150	165	146	**130**	146	142	145	130	140					
36′·0	31	162	28	0	20	175	0	152	125	130					
46′·0		0	5	125	120	150	155	165	130	120	130				
56′·0		42	161	130		42		11	126	125	110				
−45° 06′·0		66		114	83	36	40	5	148	154	165	5			
16′·0		30	165	136	110	62	62	62	44			102?			
26′·0	9	4	173	173	147	64	74	74	74	105	112	112	112	112?	112?
36′·0		10	10	5		95	72	80	80	90	100	110	110		
46′·0						80	**72**	72	**72**	87	80	97			
56′·0								88	81	91		96	101	135	136
−46° 06′·0									88			93	126	148	133
16′·0													161		

TABLE 5 (*Continued*)

(*b*) *Central Region*

Declination* 1950.0	Right Ascension 1950.0																	
	$13^h 20^m$			$13^h 21^m$			$13^h 22^m$			$13^h 23^m$			$13^h 24^m$			$13^h 25^m$		
−41° 56′ (a)	155			150			167			9			25					
−42° 06′ (b)	145		153	156		168	8		9	16		24	26		26	25		
−42° 11′ (b)	140		162	162		162	0		3	15		23	23		36	56		56
−42° 16′ (b)	9		9	157		177	4		9	16		24	29		28	37		50
−42° 21′ (c)			147	145	157	164	170	171	2	9	13	19	22	30	38	52	52	71
−42° 26′ (b)						158	168		0	6		11	16		31	34		34
−42° 31′ (b)	165			175		160	168		165	177		5	158		25	56		
−42° 36′ (d)					174	3	15	110	112	105	0	170	168	3	178			
−42° 39′·3 (d)						10	15	120	102	92	90	10	15	10				
−42° 42′·6 (d)						155	170	80	103†	100	95	105						
−42° 46′·0 (d)						150	145	50	100	110	125	15						
−42° 49′·3 (d)							175	155	136	125								
−42° 52′·6 (d)							170	165	155	20								
−42° 56′·0 (d)					120		3	3	168									

* Position angles tabulated at (a) 20 s, (b) 20 and 50 s, (c) 15, 35, and 55 s, (d) 0, 20, and 40 s after indicated minute of right ascension.

† Position angle for point A in Figure 7.

localized ridge of weak polarization is seen to overlap the south-preceding source, but, as this ridge shows elongation in a north–south direction greater than the known dimensions of the south-preceding source, its coincidence with the source may be fortuitous. The continuity of polarization orientation from here to the area north of the central sources suggests that this ridge is in fact a local intensification of the extended region of polarized emission in which the central sources are situated.

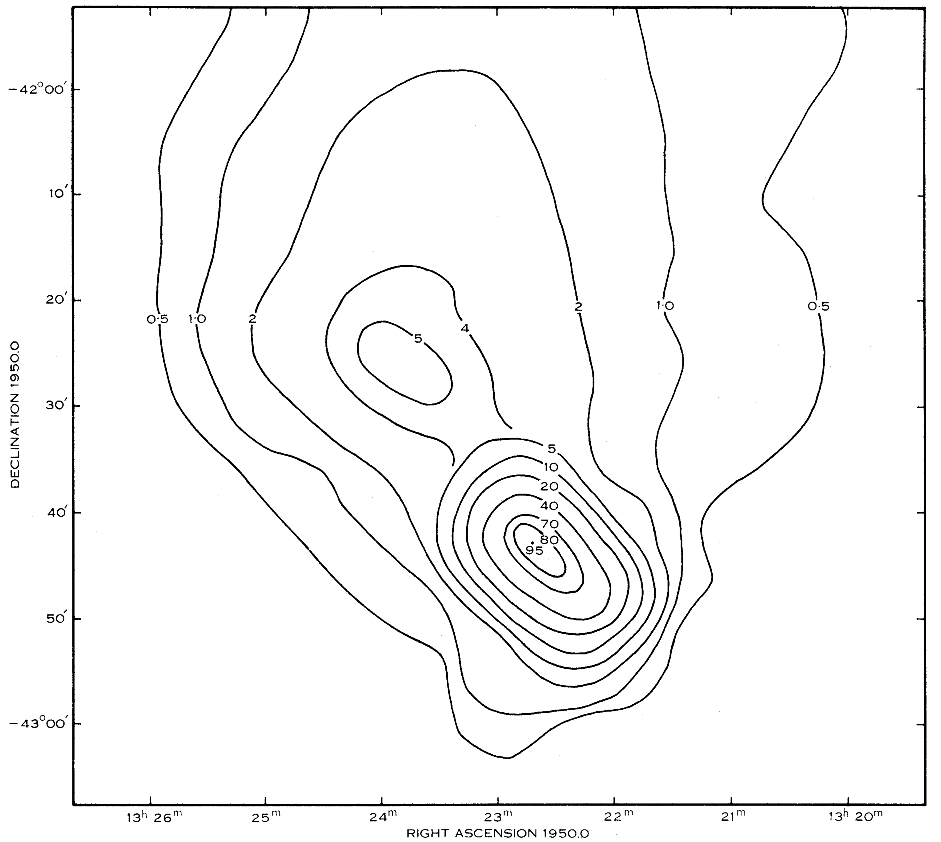

Fig. 7(*a*).—Isophotes of full-beam total emission brightness temperature at 2650 Mc/s for the central region of Figure 6.

Morris, Radhakrishnan, and Seielstad (1964), using a twin 90 ft interferometer at 2840 Mc/s, concluded that the south-west source was 5% polarized at this frequency. We are led to the conclusion, however, that the source is not more than 3% polarized in this frequency range; and we would emphasize the complexity of the polarization in the immediate vicinity of the source.

The isophotes in the central region are consistent with a double source having unpolarized components each of flux density 95 flux units, while the polarized contribution from the north-following source augments its total flux density to 108 flux units.

Beyond the central region there is very little improvement in the total intensity detail seen with the 7′·4 beam as compared with the 14′ beam at 1410 Mc/s. However, there are some regions, particularly near declination −45°, where the polarization orientation is changing rapidly and the polarization can therefore be followed more satisfactorily with the 7′·4 beam.

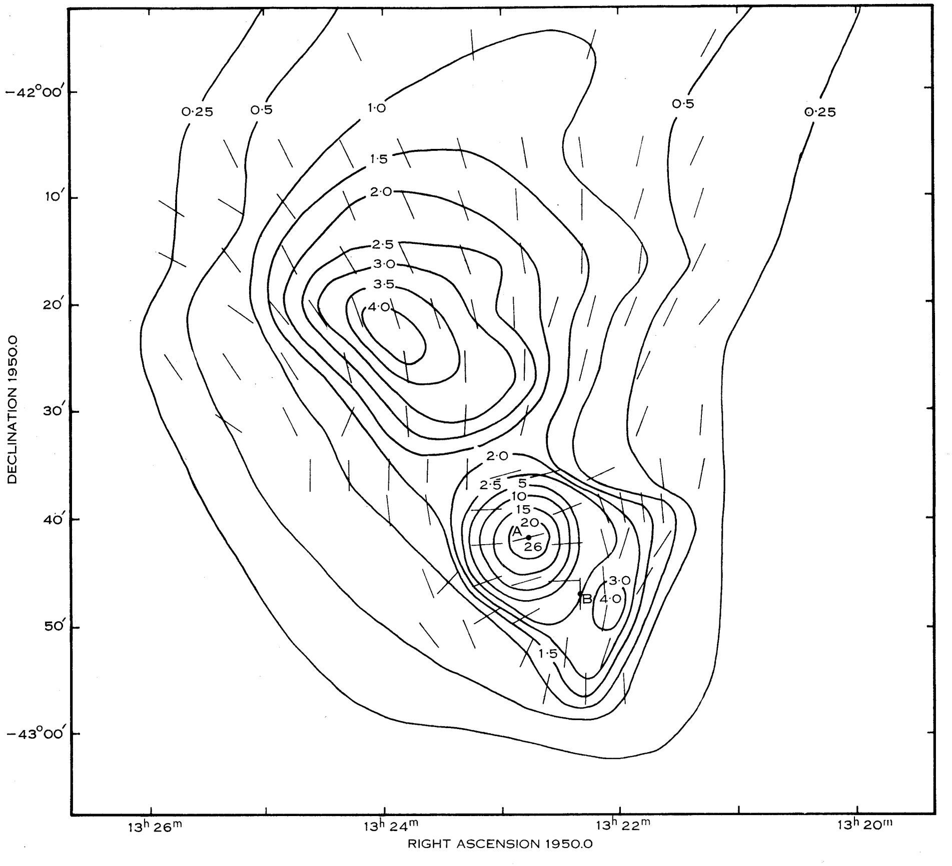

Fig. 7(*b*).—Isophotes of full-beam polarization brightness temperature at 2650 Mc/s. Short lines indicate the observed directions of the *E* vectors. The centres of the bright central sources are indicated by A and B on the map.

The dimensions of the secondary maximum centred at declination −42° 30′ can be determined with some accuracy by subtracting the emission of the central component. This secondary source falls to half intensity in a distance of approximately 15′ from the maximum intensity in the east, south, and west directions and merges in the north with the remainder of the northern extended source.

VIII. Observations at 6 cm

Limited observations of the central double source have been carried out at a wavelength of 6·0 cm. For these observations a crystal mixer receiver of 650°K double sideband noise temperature and a 10 Mc/s bandwidth was used. With a 2 s time constant the peak-to-peak fluctuations were 1·5 degK in aerial temperature.

This sensitivity was adequate for observing the central sources but not for the extended source. The beamwidth at half intensity was $4' \cdot 1$ so that the central sources were well resolved. This is illustrated by Figure 8, which shows scans made along a track passing close to the centres of the double source. Scan (*a*) was made with the feed horn oriented to give maximum reception of the polarized component in the north-following source, while scan (*b*) was made with the feed in the orthogonal orientation to give minimum reception of the polarized component. From scans such as these it was determined that the unpolarized components of the double source are almost equal in intensity and are elongated along the line joining them,

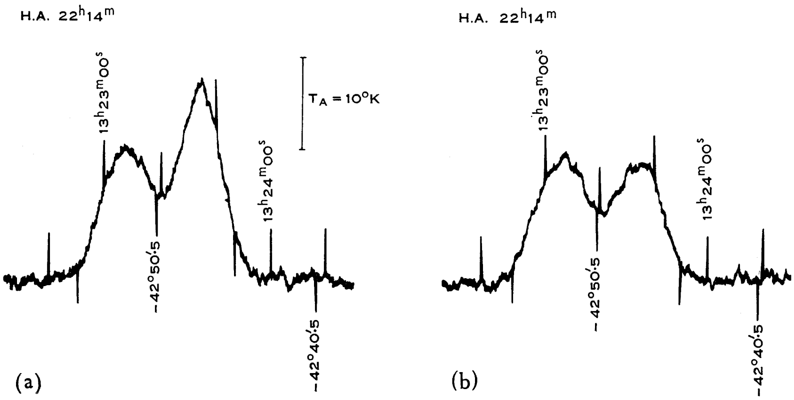

Fig. 8.—Scans through the central double source of Centaurus A at 5000 Mc/s. (*a*) Feed horn oriented for maximum signal from the north-east (right-hand) source; position angle of *E* vector 132°. (*b*) Feed horn oriented for minimum signal from this source; position angle of *E* vector 42°.

as suggested by Maltby (1961). The amount of beam broadening is consistent with equivalent Gaussian source widths of $3' \cdot 5$ in position angle 45° and 2′ in position angle 135° (the transverse direction). The polarized region of the north-following source is noticeably smaller than the unpolarized region, and its equivalent Gaussian diameter is not more than 2′. This is consistent with measurements made with an interferometer at 10·6 cm by Morris, Radhakrishnan, and Seielstad (1964).

Observations made with the rotating feed showed that the north-following source is $18(\pm 2)\%$ polarized in position angle $132°(\pm 5°)$, while the south-preceding source is $3(\pm 1 \cdot 5)\%$ polarized in position angle $103°(\pm 10°)$. These percentages are not corrected for resolution effects, and the actual percentage polarization in the polarized region of the north-following source must be considerably higher than 18%.

The 6·0 cm flux density of the north-following source is calculated to be 71 flux units and that of the south-preceding source to be 55 flux units. The probable error of these flux densities may be as high as 25%, due partly to uncertainties in the flux densities of calibrator sources and partly to a zenith-angle dependence of aerial gain, which made accurate intercomparison of source intensities difficult.

IX. Intrinsic Structure and Polarization

Figure 9 shows the intrinsic structure of the source as deduced from the present series of observations and supplemented by other published interferometric data for the central component. The contours represent equally spaced intensities in arbitrary units (dashed contour is one half unit in value). Since the spectral index is essentially constant throughout the wavelength range $3 \cdot 5$ m to 11 cm, and possibly down to 6 cm, the map should also be applicable throughout this range. An inset enlarged by a factor of five shows the central double source in relation to the optical disk of NGC 5128. Position measurements in which the pointing errors of the telescope were determined as accurately as possible by reference to identified sources gave the following position for the central component:

	R.A. 1950.0	Declination 1950.0
North-following source	$13^{h}\,22^{m}\,47^{s}\cdot 0 \pm 2^{s}$	$-42^{\circ}\,42'\cdot 5 \pm 0'\cdot 5$
South-preceding source	$13^{h}\,22^{m}\,20^{s}\cdot 5 \pm 2^{s}$	$-42^{\circ}\,47'\cdot 4 \pm 0'\cdot 5$

The two sources lie on a line in position angle $44^{\circ} \pm 1^{\circ}$ at a spacing of $6'\cdot 8 \pm 0'\cdot 2$. Their positions are approximately, but not quite, symmetrically placed with respect to the optical disk of NGC 5128. Bracewell (personal communication) has reviewed available positional data for NGC 5128 and has given a position for its optical centre as:

R.A. 1950.0 $13^{h}\,22^{m}\,31^{s}\cdot 6 \pm 0^{s}\cdot 5$ Declination 1950.0 $-42^{\circ}\,45'\cdot 4 \pm 0'\cdot 1$

Thus the mid point of the radio sources appears to be displaced approximately $0'\cdot 5$ to the north and by 2^{s} of R.A. to the east of the optical centre of NGC 5128. It should be noted that the accurately known position calibrators were at a considerable distance from Centaurus A, and the displacement quoted above should, for the present, be regarded as barely significant in relation to the probable errors.

Intrinsic polarization position angles and Faraday rotation measures were determined for as many points as possible in the source, as described in Section X. The polarization position angles are listed in Table 6. In Figure 9, vectors have been drawn at right angles to the intrinsic polarization E vectors to show the projected orientation of the magnetic field at the source. The numbers on the map are Faraday rotation measures in radians per metre squared and are negative in value.

The source appears to consist of a number of ejecta that have originated in NGC 5128 and have streamed away from it in a very open spiral. The initial direction of motion on the north side is towards the north-east, changing in the space of about half a degree to a general northerly direction and maintaining this up to the northern boundary of the source. On the south side, the spiral changes direction by about 90° in a more gradual fashion, starting in a south-westerly direction and finishing in a south-easterly direction. A high degree of symmetry is shown in the size and placing of the central components on the periphery of NGC 5128 and in their approximately equal flux densities, but this structural symmetry is not maintained in the outer extensions, although, as has been noted earlier, the total power emission is very evenly divided between the northern and southern regions. Apart from this lack of symmetry, the well-defined intensity maximum near declination $-42^{\circ}\,30'$ may be paired off with the broad maximum at $-44^{\circ}\,20'$, and the weak feature at declination

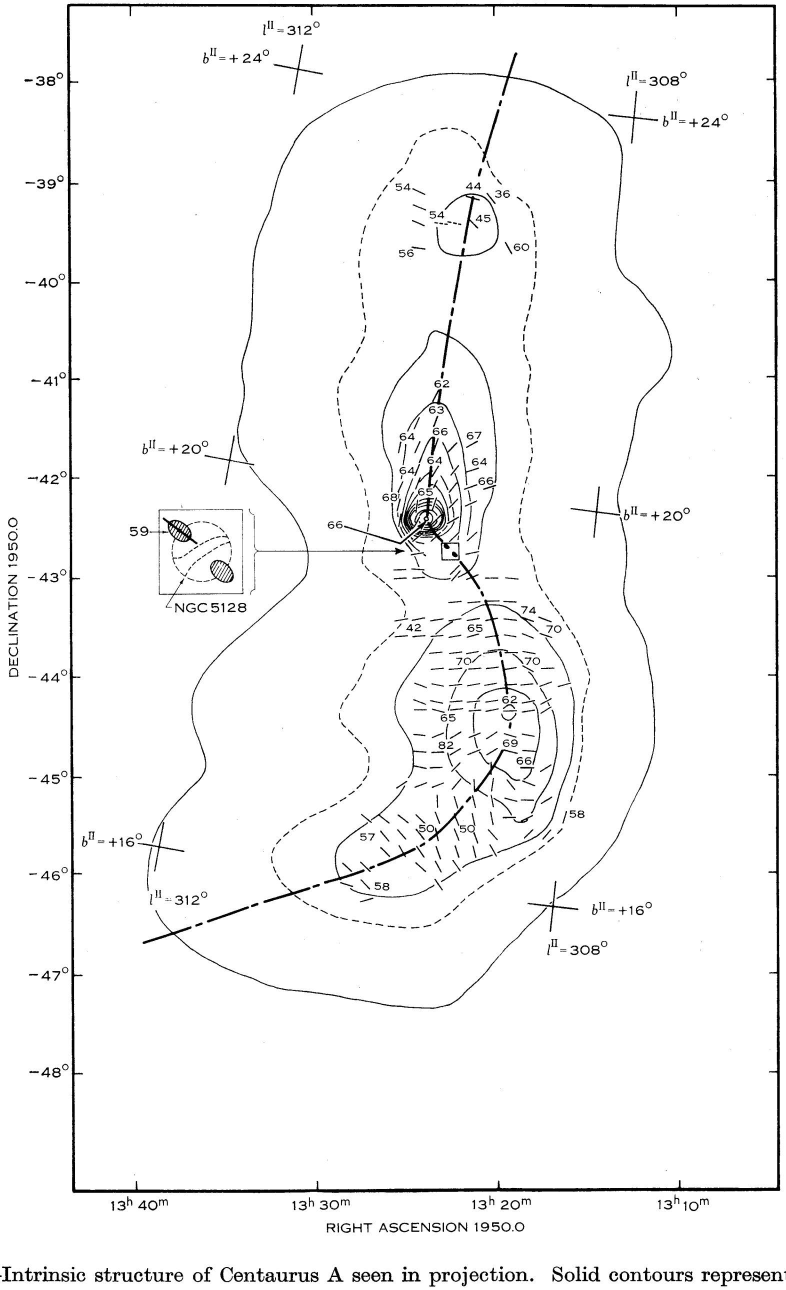

Fig. 9.—Intrinsic structure of Centaurus A seen in projection. Solid contours represent equally spaced values of intensity in arbitrary units (dashed contour is one half unit in value). Enlarged inset shows central components (shaded) in relation to NGC 5128. Vectors are at right angles to the intrinsic E vectors of the source to indicate the direction of the projected magnetic field at the source. Numbers indicate magnitudes of Faraday rotation measures, negative in sign in all cases. The heavy broken line shows the ridge line of the source.

TABLE 6

CENTAURUS-A INTRINSIC POLARIZATION POSITION ANGLES IN DEGREES

Add 20 s to indicated minute of right ascension

Declination 1950.0	Right Ascension 1950.0													
	$13^h 16^m$	17^m	18^m	19^m	20^m	21^m	22^m	23^m	24^m	25^m	26^m	27^m	28^m	29^m
−38° 26′								0						
56								153						
−39° 11′					135	171	174	5						
26				82	148	130	172	142						
41		115	115	120				135	155					
56		115	115											
−41° 11′								62						
26									66					
41						30	46	75		80				
56′						20	42	52	68					
−42° 11′					0	23	41	61	75					
16				20	10	25	53	60	73	70				
26							30	55	60	80				
36						40	160	40	40					
41							147*							
46						10			5					
−43° 01′				175	0	23	50		175	15				
26			170	177	7	175	170	0	8	8				
36	165	158	161	174	15	8	5	5	10	10				
46	165	168	166	13	18	13								
56		177	17	4	4	2	0							
−44° 11′					5	5								
21	15	30	4	178	8	8	11							
36	30	80	50	173	55	55	40							
46	54	174	169				20	10						
56			163	163				6						
−45° 26′	40	33	34	7	92	107	102	102	145	152	152	152		
41	50	50	45		122	97	107	107	130	140	140	150		
56							125	120	130		132	145		
−46° 06′													12	177
16											135	4		

* North-following central source.

$-39^\circ 30'$ with the feature near declination $-46^\circ 00'$. The latter may well have been a separate feature at an earlier stage in the development of the source.

The polarization of the source shows considerable variety, both in uniformity and orientation relative to the spiral structure. In view of the prevalence of strong polarization elsewhere in the source, it is surprising that the south-preceding central source is so weakly polarized. It is possible that the magnetic field in this source is relatively disordered at its present stage of development.

Alternatively, the three-dimensional structure of the source may be such that the north-following source lies partly in front of NGC 5128 while the south-preceding source lies partly behind NGC 5128. Differential Faraday rotation in the outer regions of NGC 5128 may then account for the depolarization.

In the north-following source there appears to be a core of strong polarization, but with presently available resolution it is not known in detail how the polarization varies across the source. However, it does appear that the polarization orientation changes suddenly by about 90° at the boundary of the north-following source.

In the region immediately north of the central component, the projected magnetic field vectors run generally along the source extension and some fanning out of the vectors may be noted. It is quite possible that this fanning out is connected with the elongation of the intensity contours in this region. North of declination $-41^\circ 00'$ the polarization is generally more confused than elsewhere in the source and it is difficult to discern any systematic pattern. On the other hand, there are some very large areas of uniform polarization in the southern extended source. For example, in the region around declination $-44^\circ 00'$ there is an area of about 2 square degrees where the field vectors are uniformly transverse. At an assumed distance of 4 Mpc this would represent a projected area of about 10^{10} square parsecs. There is a region of confused polarization near declination $-45^\circ 00'$, which divides the above region from a region around declination $-46^\circ 00'$ where the field vectors again become transverse to the spiral axis. This division lends additional support to the suggestion that the two regions in question have partly intermingled after being originally separate.

The integrated polarization of the whole source is of some interest for comparison with other unresolved sources. This integration has been done at 21 cm where the polarization data for the source are reasonably complete. The source was divided into small areas over which the polarization was substantially uniform. By adding up the Stokes "Q" and "U" parameters for these regions the integrated degree of polarization was determined to be approximately 7% with the E vector in position angle 38°. Since the polarization data were less complete at 31 and 11 cm, the integrated polarization was not determined at these wavelengths. However, taking an average Faraday rotation of 150° for the whole source at 21 cm, the intrinsic position angle for the integrated polarization would be approximately 8°.

X. Faraday Rotation

The rotation of the position angle of the electric vector with a wavelength squared dependence, the well-known phenomenon of Faraday rotation, has already been noted at three points in the source (Cooper and Price 1962). Subsequent determination

TABLE 7

CENTAURUS-A FARADAY ROTATION MEASURES

Values in units of rad/m². Add 20 s to indicated minute of right ascension

Declination 1950.0	Right Ascension 1950.0											
	$13^{h}16^{m}$	17^{m}	18^{m}	19^{m}	20^{m}	21^{m}	22^{m}	23^{m}	24^{m}	25^{m}	26^{m}	27^{m}
−38° 26′								53				
−38° 56′								48				
−39° 11′					36	45						
−39° 26′						42	53	54	54			
−39° 41′				60				29	54?			
−40° 56′												
−41° 11′								64				
−41° 26′								63				
−41° 41′						68	67	67	65			
−41° 56′						64	64	64	64			
−42° 11′					67	66	63	66	69			
−42° 41′								59*				
−43° 26′			75	74					42	42	35	
−43° 41′		70				66			41			
−43° 56′			71	71	71	71	71					
−44° 21′			63	63	63		65					
−44° 41′				70				84				
−44° 56′			67	67								
−45° 26′	58				51	51	51	51				
−45° 41′					51	51	51	51			58	
−45° 56′												59
−46° 16′												59

* North-following central source.

of the polarization parameters over the entire source at several wavelengths have enabled us to study the Faraday rotation characteristics over a region of approximately 12 square degrees in the more intense regions of the source.

Using polarization data from 31, 21, and 11 cm surveys, the electric vector position angles for each point investigated were plotted as a function of wavelength squared. These plots gave the intrinsic polarization angle, by extrapolation to zero wavelength, and the rotation measure (as defined by Gardner and Whiteoak 1963) for each point. For each position angle there was an ambiguity of $n\pi$, and a best fit to the position angle versus wavelength squared plot was effected, accepting the lowest rotation measure consistent with the observational data. Values of rotation measure were derived for some 63 points distributed over the entire source, taken in regions where the total brightness and the polarization brightness allowed a good signal-to-noise ratio in the observations.

Table 7 lists these rotation measures in units of radians per metre squared, and a representative number of them are included in Figure 9.

The origin of the Faraday rotation in this and other radio sources has been the subject of previous discussion (Cooper and Price 1962; Sciama 1962; Gardner and Whiteoak 1963; Gardner 1964) and it is now generally accepted that the rotation occurs in the galactic halo. It is possible that a small amount of Faraday rotation occurs in the source itself, but from depolarization considerations, as discussed in Section XII, the amount of rotation occurring in the source can only be a small fraction of the observed total.

To account for a rotation measure R.M. we need an electron density and magnetic field such that

$$\text{R.M.} = 8\cdot 1\times 10^5 \int N_e H_l \, \mathrm{d}l,$$

where N_e is the electron density in electrons/cm^3, H_l is the longitudinal component of the magnetic field in gauss, and $\mathrm{d}l$ is an element of path length measured in parsecs. Estimates of the path length over which the Faraday rotation may be occurring range from a few hundred parsecs to about 10 kpc. For the short path length, electron densities of $\sim 10^{-2}$ electrons/cm^3 and magnetic fields of $\sim 10^{-5}$ G are indicated, while for the longer path length the field strength and electron density may be reduced accordingly.

Since Centaurus A provides by far the largest continuous area of extragalactic polarization, it affords a unique opportunity to study the scale on which rotation measures, and hence magnetic field strengths and electron densities, vary in the galactic halo. This is the more so since it has turned out that a specially interesting span of galactic latitude is covered. It may be seen from Figure 9 that the rotation measures tend to maximize near $b^{\mathrm{II}} \simeq +18°$ and fall off in an irregular manner towards the northern and southern boundaries of the source at $b^{\mathrm{II}} = +24°$ and $+16°$ respectively. The fall-off at lower and higher latitudes is consistent with the conclusion reached by Gardner and Davies (personal communication) from a general study of galactic Faraday rotation that, in the vicinity of $l^{\mathrm{II}} = 310°$, the rotation measure passes through zero and changes sign at $b^{\mathrm{II}} \simeq +10°$ and $+50°$.

In more than half of the Centaurus-A area where rotation measures have been obtained, the value does not change more than 10–15% in the space of a degree, but some small regions may be noted in Figure 9 where a change of the order of 30% in rotation measure occurs in the space of one-quarter to one-half of a degree. The boundaries of these regions are revealed in several places on the 31 cm polarization map of Figure 3 by the lack of polarization due to differential Faraday rotation across the telescope beam.

In regions of fairly uniform rotation measure the estimated accuracy is $\pm 5\%$. For points that have been given special study, such as the central component, the point at right ascension $13^{\mathrm{h}}\,24^{\mathrm{m}}$, declination $-42^{\circ}\,30'$, and the point at right ascension $13^{\mathrm{h}}\,20^{\mathrm{m}}$, declination $-42^{\circ}\,25'$, the accuracy is estimated to be $\pm 2\%$.

XI. Spectral Analysis

Flux densities derived in previous sections are summarized in Table 8 and a logarithmic plot of these flux densities is presented in Figure 10 together with other published data on Centaurus A. At frequencies below our lowest value of 406 Mc/s the most recent data are those of Sheridan (1958) at 85 Mc/s and Shain (1958) at 19·7 Mc/s.

Table 8

CENTAURUS-A FLUX DENSITIES AT SEVERAL WAVELENGTHS

Values in units of $10^{-26}\,\mathrm{W\,m^{-2}\,(c/s)^{-1}}$

Wavelength (cm)	Total Emission	Central Component Emission	Extended Component Emission	
			North	South
74	2740	595 (22%)	1075 (39%)	1070 (39%)
31		370		
21	1330	288 (22%)	510 (38%)	532 (40%)
11		203		
6		126		

The plot of total source flux density (curve 2) indicates strong curvature of the spectrum, with an index of approximately $-0\cdot9$ at the low frequency end, decreasing to $-0\cdot6$ at the high frequency end. On the other hand, the plot for the central component (curve 1) shows a fairly uniform average slope with an index of $-0\cdot6$. If the 85 Mc/s flux densities are multiplied by 0·82, as has been suggested by Kellermann (1964) to harmonize the flux scale of the 85 Mc/s survey of Mills, Slee, and Hill (1958, 1960) with the currently accepted flux scale for northern sources, the resulting 85 Mc/s flux densities for the whole source and for the central component fall quite close to a straight line plot through our higher frequency data. The rise in total flux density at 19·7 Mc/s then becomes even more pronounced, but in the absence of independent measurements in the 19 Mc/s region we are unable to assess the reality of this rise. The uncertainty of the 19·7 Mc/s absolute intensity scale was estimated by Shain to be up to 20%. However, the assessment of the proportion of the total emission that is contributed by the central component should be subject to much smaller uncertainties, and we note that this proportion decreases from 22% at frequencies of 85 Mc/s and above to 11% at 19·7 Mc/s. This decrease may possibly be explained by the mechanism, which has been discussed by Kellermann (1964), whereby, in the early life of certain sources, the rate of injection of energetic particles has not come into equilibrium with the radiation losses. In such a case the spectral slope is expected to flatten towards the low frequency end, but as the source ages and equilibrium is reached the spectral curvature disappears. Thus the central component of Centaurus A may be at such an early stage of development, while the outer parts have reached equilibrium.

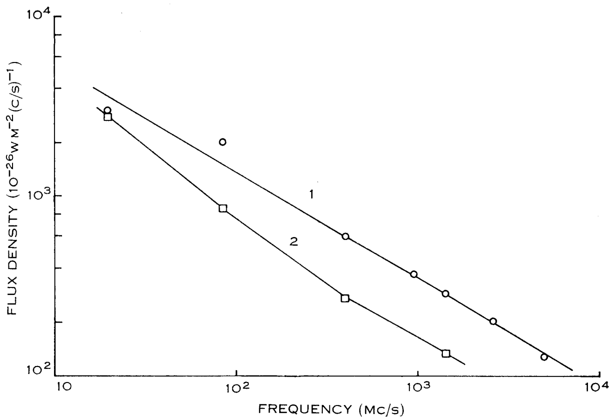

Fig. 10.—Spectrum of the total emission of Centaurus A, curve 2 (÷ 10), and the central component emission, curve 1, plotted from the data of Table 7 together with data at 19·7 Mc/s from Shain (1958) and at 85 Mc/s from Sheridan (1958).

A value of 1765 flux units for the combined emission of the central component and the northern and southern parts of the extended source at 960 Mc/s has been given by Bolton and Clark (1960). Recent adjustments to the Caltech flux density scale indicate that this value should be multiplied by 0·95, bringing it closely into line with our own flux density for this frequency. The same authors estimated a flux density for the central component of 460 flux units at 960 Mc/s, but they appear to have overestimated the contribution of the central component to their isophotes, which were observed with a 0°·8 beam. In the light of our improved knowledge of the source structure, a value of 370 flux units seems more reasonable.

XII. Depolarization Effects

As the observing wavelength increases, a number of effects come into play to decrease the degree of polarization observed in the source. Firstly, the larger beam may encompass areas of differing polarization orientation with the result that the net polarization decreases. The differing polarization orientations may be inherent in the source or may be due to differential Faraday rotation between the source and the observer. The latter effect certainly operates in some areas of Centaurus A.

Even in areas of uniform polarization there may be depolarization due to Faraday rotation occurring in the source along with the emission process. If the emission and rotation are uniformly distributed in depth through the source and the radiation from the most distant part of the source is subjected to a total rotation of x degrees before emerging from the source, it may readily be shown that there will be a net Faraday rotation of $\frac{1}{2}x$ degrees for the integrated emission, and a depolarization factor $(\sin x)/x$ applicable to this emission. Thus depolarization will become very pronounced as x approaches 180°. A uniform distribution of rotation with depth in the source is not to be expected in practice, but for more tapered distributions the depolarization factor will still be much the same for a given total Faraday rotation.

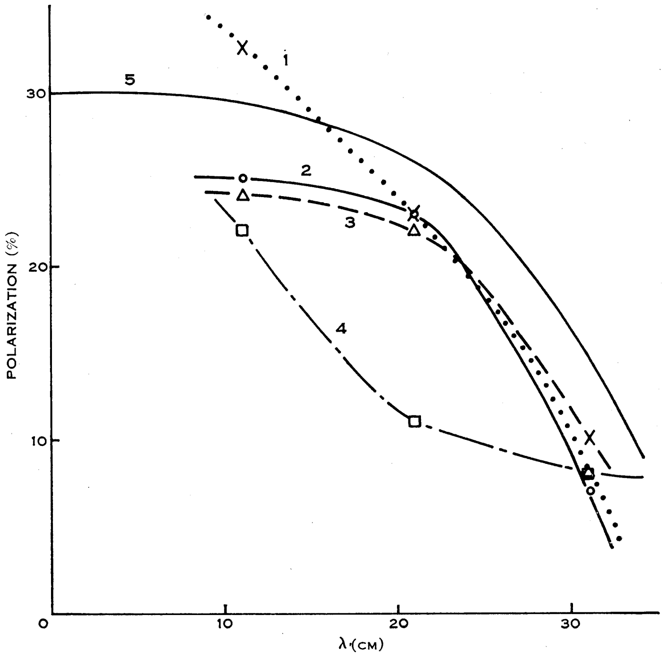

Fig. 11.—Plots of the percent polarization at several points in Centaurus A as a function of wavelength: curve 1, R.A. $13^h 22^m$, dec. $-43° 45'$; curve 2, R.A. $13^h 24^m$, dec. $-41° 15'$; curve 3, R.A. $13^h 21^m \cdot 5$, dec. $-44° 25'$; curve 4, R.A. $13^h 21^m \cdot 5$, dec. $-45° 30'$; curve 5, a plot of the function $P_0(\sin R\lambda^2)/R\lambda^2$, where $P_0 = 30\%$ and $R = 20$ rad/m^2.

In an attempt to set a limit to the amount of Faraday rotation occurring in Centaurus A, the variation in percent polarization with wavelength is plotted in Figure 11 for four regions where confusion effects in the beam are small at wavelengths up to 31 cm. For comparison a plot of the depolarization to be expected due to a rotation measure of 20 rad/m^2 distributed uniformly in depth through the emitting region is shown in Figure 11, curve 5. This plot has been arbitrarily drawn for 30% polarization at zero wavelength.

Curve 5 suggests that the upper limit for the internal rotation measure of the source is about 20 rad/m^2 and therefore that the net rotation in the source has an upper limit of about 10 rad/m^2, that is, about one-sixth of the observed rotation.

XIII. Extraneous Sources

In the course of the observations two extraneous sources of moderate intensity were discovered within the boundaries of Centaurus A, and a third was discovered just outside the south-preceding extremity of Centaurus A. These sources are listed in Table 9 in order of increasing right ascension. The resolution at 74 cm wavelength was not sufficient to distinguish any of these sources, but the first and second were quite clearly defined at 21 cm. The third source was only distinguishable at 11 cm.

Table 9

Extraneous sources in the Centaurus-A region

Source:	1315–46	1318–43	1320–44
Position (1950.0)			
Right ascension	$13^h 15^m 35^s$	$13^h 18^m 13^s$	$13^h 20^m 07^s$
Declination	$-46° 05'{\cdot}5$	$-43° 26'{\cdot}3$	$-44° 35'{\cdot}1$
Annual precession			
$\Delta\alpha$ (s/yr)	3·53	3·49	3·52
$\Delta\delta$ ($'$/yr)	−0·32	−0·32	−0·31
Flux density			
(10^{-26} W m^{-2} (c/s)$^{-1}$)			
1410 Mc/s	2·65	5·8	—
2650 Mc/s	1·32	4·75	1·45
Spectral index			
1410 → 2650 Mc/s	−1·0	−0·31	—
Angular size			
N.–S.	P	$5'{\cdot}0$	P
E.–W.	P	$6'{\cdot}3$	P
Degree of polarization			
at 1410 Mc/s	$< 3\%$	See text	See text

The source 1318–43 has equivalent Gaussian dimensions of $4'{\cdot}5 \times 6'{\cdot}3$ and is identified with an elliptical galaxy of approximately $14^m{\cdot}5$ found on a plate taken by Dr. J. B. Whiteoak with the Mt Palomar 48 in. Schmidt telescope. Within the position error rectangle of 1320–44 no nebular images can be distinguished to the plate limit, and there are no stellar images brighter than about 17^m. The position of the source 1315–46 has not been examined yet, as no high definition plates are available for the region.

The source 1315–46 is less than 3% polarized at 21 cm and the other two sources show no polarization that can be distinguished from the strong polarization of Centaurus A and of the foreground, which surrounds them.

XIV. Conclusions

The work described here has revealed Centaurus A as a unique object for studying the processes by which radio galaxies evolve. Its polarized emission enables the distribution of magnetic fields to be traced over the extremely large volume of space occupied by the source, while at the same time allowing the details of galactic Faraday rotation to be traced over a particularly interesting region of the sky.

POLARIZATION OF CENTAURUS A

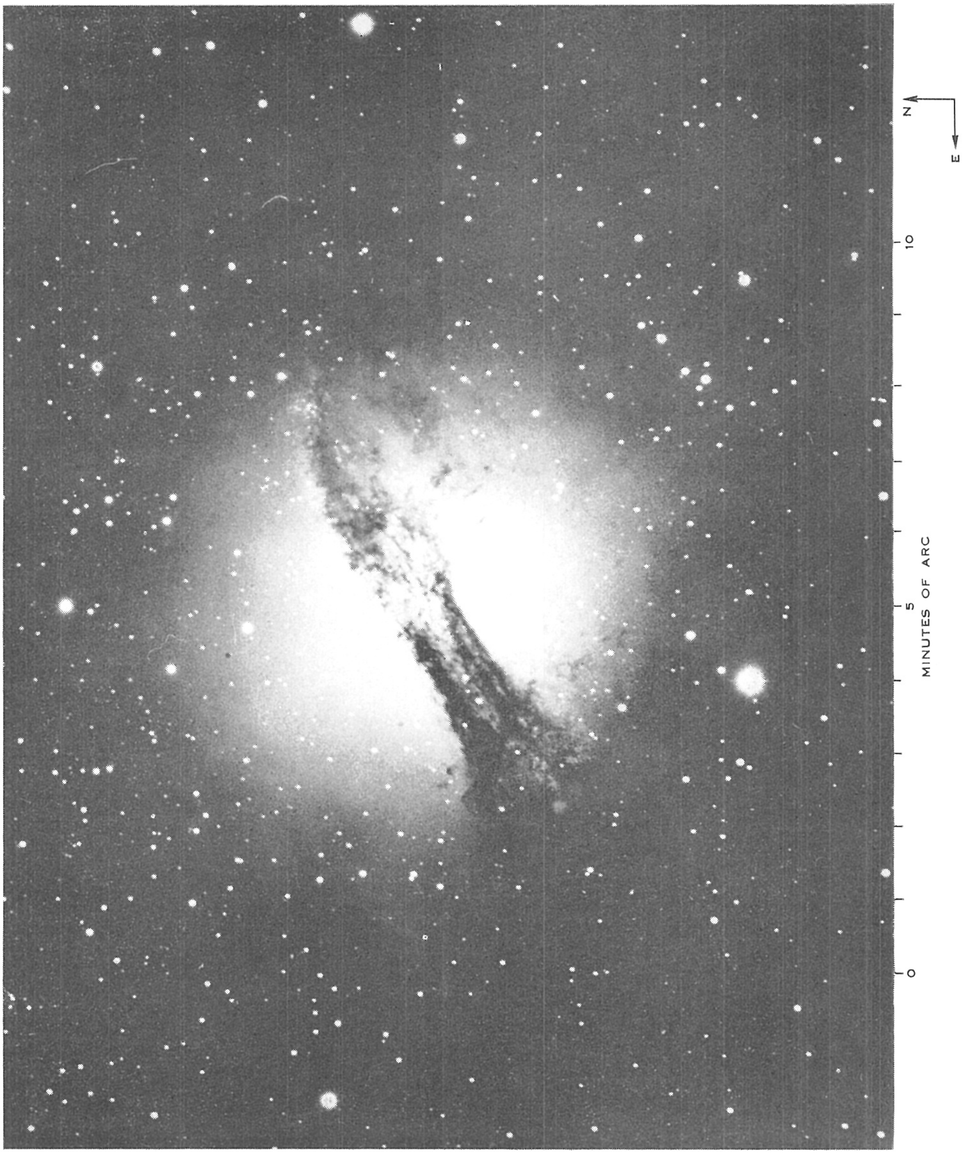

NGC 5128. From the Hubble Atlas of Galaxies, Carnegie Institute of Washington, 1961. (Note that the orientation of the galaxy given in the Hubble Atlas is incorrect.)

The basic features of the source and the Faraday rotation are now apparent, and it remains for further studies employing higher sensitivity and resolution to build up a more detailed picture. Observations that will be of special interest concern the polarization of the south-preceding central source at wavelengths below 6 cm, and the regions in the extended source where the Faraday rotation appears to be changing rapidly. A definite answer to the question, whether or not Centaurus A extends further on its south-following side than we have assumed in the present paper, is also needed.

XV. Acknowledgments

We thank Mr. J. G. Bolton and Dr. F. F. Gardner for critical readings of the manuscript and for their helpful suggestions on points of interpretation. One of us (R.M.P.) is at present the holder of a National Science Foundation Fellowship.

XVI. References

Bolton, J. G. (1948).—*Nature* **162**: 141.
Bolton, J. G., and Clark, B. G. (1960).—*Publs Astr. Soc. Pacif.* **72**: 29.
Bolton, J. G., Stanley, G. J., and Slee, O. B. (1949).—*Nature* **164**: 101.
Bolton, J. G., Westfold, K. E., Stanley, G. J., and Slee, O. B. (1954).—*Aust. J. Phys.* **7**: 96.
Bracewell, R. N., Cooper, B. F. C., and Cousins, T. E. (1962).—*Nature* **195**: 1289.
Burbidge, E. M., and Burbidge, G. R. (1959).—*Astrophys. J.* **129**: 271.
Conway, R. G., Kellermann, K. I., and Long, R. J. (1963).—*Mon. Not. R. Astr. Soc.* **125**: 261.
Cooper, B. F. C., Cousins, T. E., and Gruner, L. (1964).—*Proc. Instn Radio Engrs Aust.* **25**: 221.
Cooper, B. F. C., and Price, R. M. (1962).—*Nature* **195**: 1084.
Elvius, A., and Hall, J. S. (1964).—*Bull. Lowell Observ.* **6**: 123.
Gardner, F. F. (1964).—Symp. IAU–URSI No. 20 (Canberra 1963). p. 143.
Gardner, F. F., and Milne, D. K. (1963).—*Proc. Instn Radio Engrs Aust.* **24**: 127.
Gardner, F. F., and Whiteoak, J. B. (1963).—*Nature* **197**: 1162.
Hindman, J. V., and Wade, C. M. (1959).—*Aust. J. Phys.* **12**: 258.
Johnson, H. M. (1963).—Pubs NRAO, Volume 1, No. 15.
Kellermann, K. I. (1964).—*Astrophys. J.* **140**: 969.
Komesaroff, M. M., and Mathewson, D. S. (1962).—*Aust. J. Phys.* **15**: 572.
McGee, R. X., Slee, O. B., and Stanley, G. J. (1955).—*Aust. J. Phys.* **8**: 347.
Mackey, M. B. (1964).—*Proc. Instn Radio Engrs Aust.* **25**: 515.
Maltby, P. (1961).—*Nature* **191**: 793.
Mills, B. Y. (1953).—*Aust. J. Phys.* **6**: 452.
Mills, B. Y., Slee, O. B., and Hill, E. R. (1958).—*Aust. J. Phys.* **11**: 360.
Mills, B. Y., Slee, O. B., and Hill, E. R. (1960).—*Aust. J. Phys.* **13**: 676.
Morris, D., Radhakrishnan, V., and Seielstad, G. A. (1964).—*Astrophys. J.* **139**: 560.
Piddington, J. H., and Trent, G. H. (1956).—*Aust. J. Phys.* **9**: 74.
Sciama, D. W. (1962).—*Nature* **196**: 760.
Sérsic, J. L. (1958).—*Observatory* **78**: 24.
Sérsic, J. L. (1961).—*Revta Univ. Nac. Córdoba* **11**: No. 3.
Shain, C. A. (1958).—*Aust. J. Phys.* **11**: 517.
Sheridan, K. V. (1958).—*Aust. J. Phys.* **11**: 400.
Stanley, G. J., and Slee, O. B. (1950).—*Aust. J. Sci. Res.* A **3**: 234.
de Vaucouleurs, G. (1953).—*Observatory* **73**: 252.
de Vaucouleurs, G. (1956).—*Occ. Notes R. Astr. Soc.* **3**: 118.
Wade, C. M. (1959).—*Aust. J. Phys.* **12**: 471.
Westerhout, G., Seeger, C. L., Brouw, W. N., and Tinbergen, J. (1962).—*Bull. Astr. Insts Neth.* **16**: 187.